JOURNAL OF AIRCRAFT
Vol. 48, No. 4, July–August 2011

Experiments with Geometric Nonlinear Coupling for Analytical Validation

Jonathan Boston,* Eric Swenson,† and Donald Kunz‡
U.S. Air Force Institute of Technology, Wright-Patterson Air Force Base, Ohio 45433
Wenbin Yu§
Utah State University, Logan, Utah 84322
and
Maxwell Blair¶
U.S. Air Force Research Laboratory, Wright-Patterson Air Force Base, Ohio 45433

DOI: 10.2514/1.C031033

This study was focused on obtaining accurate experimental data for the validation of the geometrically exact beam theory from a series of experiments in which high-quality surface shape and deflection data were collected. Many previous experiments have experienced issues with data collection or test articles, which the researchers were unable to overcome. This test program was performed in two stages: qualification and joined wing. The qualification stage validated the experimental procedures on a simple 72-in.-long aluminum beam with 8 in. × 0.5 in. cross section. The joined-wing stage was the primary experiment focused on obtaining quality data for use in validation, and each joined-wing test article had an overall length of 57 in. The fore wing segment was designed with a chord of 8 in. and a thickness of 0.5 in.; the aft wing segment was designed with a chord of 6 in. and a thickness of 0.5 in. These dimensions were chosen so the joined-wing test article produced nonlinear bend–twist coupling before permanent deformation. Bend–twist coupling in a solid cross-section aluminum joined-wing test article was successfully captured with surface shape, deflection points, and strain data.

Nomenclature

E	=	Young's modulus, psi
g_x	=	grid point, x-direction position, in.
g_y	=	grid point, y-direction position, in.
g_z	=	grid point, z-direction position, in.
h	=	width, in.
l	=	length, in.
n	=	number of measurement points
P_{cr}	=	critical buckling load, lb
s_x	=	surface point, x-direction position, in.
s_y	=	surface point, y-direction position, in.
s_z	=	surface point, z-direction position, in.
t	=	thickness, in.
ν	=	Poison's ration

I. Introduction

THE joined-wing concept is being evaluated by the U.S. Air Force Research Laboratories (AFRL) for use in high-altitude long endurance (HALE) intelligence, surveillance, and reconnaissance (ISR) aircraft, similar in design to the Boeing SensorCraft, represented in Fig. 1. The joined-wing concept was patented by Wolkovich [1], who in 1986 presented his concept as a viable alternative to conventional aircraft designs. He cited lightweight and high wing stiffness among the chief benefits. Many researchers have and still are working on analyzing and optimizing his initial concept.

While significant work has been performed analytically and aerodynamically on the joined-wing design, experimental validation of the structural response is lacking. Part of this lack of experimentation stems from the difficulty of performing the experiment and the fidelity of current analytical tools. When optimizing a joined-wing aircraft design, the unique bend–twist couplings inherent in the structure require nonlinear analyses. Analytical tools are being created using a newer beam theory which has shown great promise to significantly decrease solution time for optimization. One of the primary tools is geometrically exact beam theory (GEBT) [2,3]. However, any new theory must be validated experimentally.

The goals of this research are to provide experimental data on geometrically simple joined-wing test articles that will allow researchers to validate analytical tools like GEBT for use in the design of joined-wing HALE aircraft, to develop a standard set of experimental procedures for testing joined-wing test articles in the lab, and to compare experimental data with analytical results obtained using traditional nonlinear analyses.

II. Background

This research was the result of several previous and ongoing research projects, including the novel joined-wing design and GEBT. In this section, the joined-wing aircraft, previous experimental work, and previous analytical work are discussed.

A. Joined-Wing Aircraft

Throughout the history of aircraft design, unique concepts have been tried by designers with the goal of better aircraft design. The joined wing is no exception; however, it was not until 1986, when Wolkovich [1] published his research into this concept, that aircraft designers started to consider seriously the joined wing. Wolkovich's research showed that a joined-wing aircraft could compete with traditional aircraft designs. Initial optimization studies showed that while there were benefits of the joined-wing concept, there were no

Presented as Paper 2010-3018 at the 51st AIAA/ASME/ASCE/AHS/ASC Structures, Structural Dynamics, and Materials Conference, Orlando, FL, 12–15 April 2010; received 23 March 2010; revision received 10 January 2011; accepted for publication 18 March 2011.

*Graduate Student, AFIT/ENY, 2950 Hobson Way. Member AIAA.
†Assistant Professor of Aerospace Engineering, AFIT/ENY, 2950 Hobson Way. Member AIAA.
‡Associate Professor of Aerospace Engineering, AFIT/ENY, 2950 Hobson Way. Associate Fellow AIAA.
§Associate Professor of Mechanical and Aerospace Engineering, UMC 4130. Senior Member AIAA.
¶Senior Aerospace Engineer, AFRL/VASA, 2210 8th Street, Bldg 146. Associate Fellow AIAA.

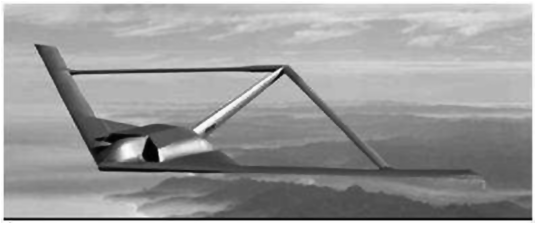

Fig. 1 Boeing SensorCraft concept [15].

direct cost savings for a midranged transport aircraft. Still, it was suggested in these studies that a different mission might provide better performance [4,5].

Roberts et al. [6], among others, is heading up work in developing the joined-wing concept for the HALE ISR aircraft, which typically need very high aspect ratio wings. However, high aspect ratio wings tend to be very flexible, especially in relatively lightweight HALE designs. The joined-wing design is proposed to allow the benefits of a high aspect ratio wing without the high flexibility normally seen with these types of aircraft.

B. Previous Experimental Work

Several studies have been performed to experimentally acquire static load data for the joined wing. Each experiment has experienced issues which the researcher was unable to overcome. Bond et al. [7] performed research in capturing the nonlinear deformations using a complex rib and spar test article. Analysis of the experimental results collected from this test article revealed rotation and translation in the assumed rigid boundary conditions. The test also revealed that the wing skins increased the stiffness to the point that the nonlinear effects were not seen, and the skins were removed for the experiment.

The second study was performed by Boston et al. [8] on a simple aluminum plate joined-wing test article produced for AFRL. Green et al. [2] had issues in tuning the finite element (FE) model to the experimental results, and concluded that the test article had been permanently deformed during the testing. This accidental permanent deformation highlighted the need to methodically rerecord the unloaded test article for data comparison and ensure that applied loads do not yield the structure.

Patil [9] tested a joined-wing configuration, but did not see nonlinear deformations before material yield. He showed that a joined wing is significantly stiffer than a single wing model.

C. Previous Analytical Work

Joined-wing concept development starts with numerical analysis. Computer simulations are a reliable substitute for ground testing if numerical methods have been experimentally validated.

Marisarla [10] constructed a FE model (FEM) with skins, ribs, and stringers. However, most of the analyses were performed assuming small (linear) deformations. Narayanan [11] used finite element analysis (FEA) to analyze an aerodynamically shaped joined-wing model and concluded that nonlinear solvers are required to accurately predict joined-wing deflections and stresses. Rasmussen et al. [12] explored design space for optimal joined-wing configuration. Nonlinear structural analysis was deemed critical in the optimization of the joined wing. Kaloyanova et al. [13] completed a simple optimization which produced a structure that did not yield under the applied aerodynamic load. Although the failure of the optimal design preluded nonlinear mechanics, nonlinear analyses were needed to arrive at the optimal design.

Patil [9] conducted analytical studies to see where and when buckling would first occur in his joined-wing design. His research points out that not all joined wings exhibit nonlinear deformations; the cross section contributes greatly to the mechanics of deformations.

Roberts et al. [6] designed a joined-wing HALE aircraft and successfully optimized the design. Although they expressed confidence in the theoretical development of the analysis tools, they noted that no experimental validation of the analytical tools had been completed and highly recommended performing experimental validation.

Adams [14] looked at the Boeing SensorCraft [15] design and developed the optimal design based on the SensorCraft design. He concluded that the initial SensorCraft design was not optimized for geometric and aeroelastic nonlinearities. His results indicated that global buckling is typically the critical condition for a weight optimized joined-wing design.

Because the time required to compute nonlinear solutions is significant, design space should be initiated with geometrically simple, but mechanically exact nonlinear methods. One approach is to model the slender members of joined wing as beams using the GEBT. Hodges [16] and Yu et al. [17] was one of the first to coalesce the various mathematical components that make up the GEBT into a coherent theory without assumptions about the way the beam deforms with relation to the beam axis or the cross section. Recently, Yu et al. [17] provided a general-purpose implementation of the mixed formulation of the GEBT into a computer code called GEBT. Work has been performed by Green et al. [2], Yu and Blair [3], and others, which uses GEBT to optimize and design joined-wing HALE aircraft. However, little experimental work has been performed to validate these design and analysis tools. Because of this lack of experimental data, this research effort is focused on collecting the experimental data necessary to validate new beam oriented analytical theories.

III. Test Design and Setup

A. Experiment Setup

This experiment was separated into two distinct stages: qualification and joined wing. The qualification stage was the first component of this experiment, and it was designed to verify all experimental procedures, resolve construction issues, and gain confidence in data collection and analysis. Because of the nature of the construction techniques and the amount of data collected and analyzed, the qualification stage was a risk reduction measure for the joined-wing stage through development of standardized experimental procedures and verification of the design. The joined-wing stage was the primary experiment of this research effort and incorporates lessons learned from procedures evaluated during the qualification stage to facilitate ease of data collection and analysis.

1. Qualification Test Article

For the qualification stage, the test article was a solid 6061 aluminum beam with a cross section of 8×0.5 in. that is 72-in.-long. The top and bottom mounting structure of the experimental test article was constructed from 4130 steel to provide rigid attachment points that are independent of the test article. The top mounting structure, Fig. 2a, provided a common cable attachment point for load application. The bottom mounting structure, Fig. 2b, held the test article fixed against unwanted movement or rotations. The load was applied through a cable system which has an integral load cell to accurately measure these loads. The forces were assumed to be applied in the direction defined by the tip of the top mounting structure and the top pulley location, as shown in Fig. 3.

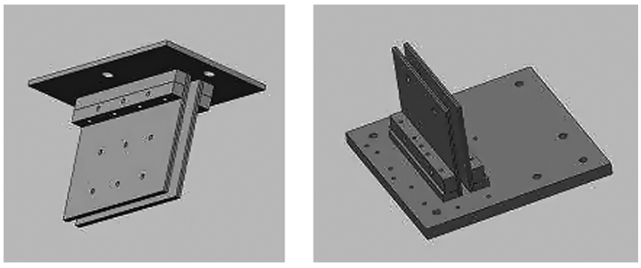

a) **b)**

Fig. 2 Mounting structure: a) top and b) bottom.

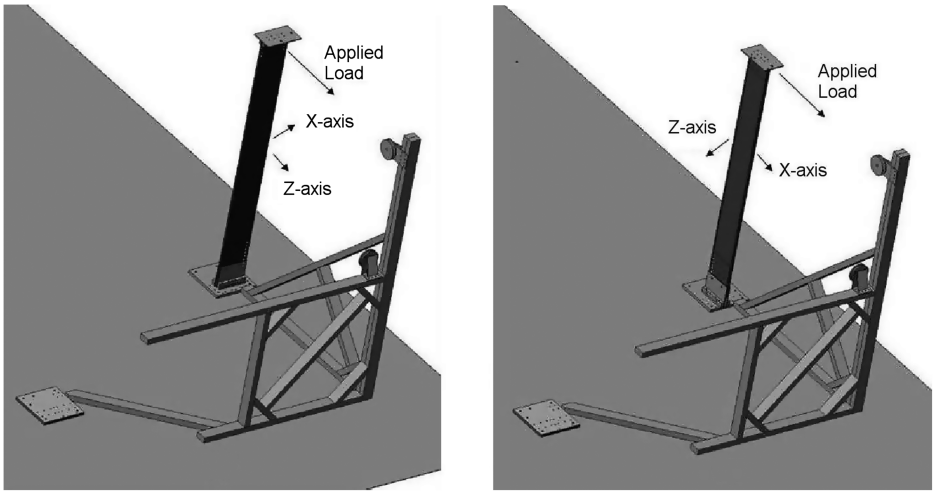

a) b)

Fig. 3 Bending around the a) lateral and b) transverse bending directions.

The qualification test article was tested in two directions, around the x and z axes, as shown in Fig. 3. Traditionally, cantilevered beams are loaded in the direction with the lowest rigidity. However, since there are nonlinear instabilities in bending along the stiffer direction that are similar to the joined wing, tests were conducted around the z axis and compared with the analytical models. In this study, the x-axis bending is referred to as lateral bending, and the z-axis bending is referred to as transverse bending.

The buckling instability in the transverse bending direction was predicted using the lateral-torsional buckling analysis as presented by Hartog [18]. The critical load before buckling in a simple cantilevered beam is calculated using:

$$P_{\text{cr}} = 4.01 \frac{Eht^3}{6l^2} \sqrt{\frac{1}{2(1+\nu)}} \tag{1}$$

where P_{cr} is the critical buckling load, E is the Young's modulus, h is the width, t is the thickness, l is the length, and ν is Poisson's ratio. For the qualification test article, the critical load before the structure buckles was calculated to be around 1000 lb, according to Eq. (1).

2. *Joined-Wing Test Design*

The second stage of the experiment consisted of a joined-wing test article. For this experiment, the goal was to provide the simplest geometry available while still notionally representing an aircraft wing.

At the structural level, a design is constrained by any number of structural design criteria. For instance, the structure must be stable and the material strong. The equivalent criteria may specify that the structure not buckle and the stress not exceed material allowables.

While joined-wing structures are commonly thought to buckle (in the sense of a static instability), they do not. It is true that joined wings are characterized by unusual compressive load paths which are normally associated with buckling, and a designer may place a buckling design criteria on the analysis model of a joined-wing concept. However, the predicted buckling load is not necessarily physically manifested with sudden explosive structural failure.

Rather, the joined-wing exhibits what structural experts call geometrically nonlinear behavior (the material remains linear). If a joined-wing designer insists on enforcing a buckling requirement, then they will design a structure that has postbuckling behavior. But, again, the structural state before and after the predicted buckling load is reached will be smoothly traversed with geometric nonlinear motion. Eventually, with a sufficiently large displacement, the material does exceed material allowables and breaks. The point here is that material allowables are not the only criteria for joined-wing structural integrity.

The joined-wing test article design makes this point clearly. The requirement for the joined-wing test article is that it demonstrates a geometrically nonlinear response before approaching material failure. These are conflicting design requirements. If the joined-wing sections are too thick, then the wing design will be strong, but will not demonstrate nonlinear behavior. If the joined-wing sections are too thin, then the wimpy wing design will immediately fall into a nonlinear state under load and will continue to curl without material failure. The dimensions of a meaningful joined-wing test article must be sized and balanced.

Therefore, the joined-wing test article was composed of two platelike beams which represented the fore and aft wing segments of the joined wing. The wing segments were constructed out of solid aluminum beams similar to the qualification test article. The height (length) of the joined-wing test article was 57 in. and the length of each wing segment was 67 in. The fore wing segment had a chord of 8 in. and the aft wing segment had a chord of 6 in. The fore and aft chord lengths were derived using trial and error optimization using nonlinear FE models to match the stresses in the roots of both wings at various load cases and especially near the yield point of the material.

As with the qualification test article, the top and bottom mounting structure (Fig. 4) were made out of 4130 steel to minimize movement in the mounting structure. Throughout all tests, the bottom mounting structure was examined to make sure no undesirable deformations or deflections occur. Since one of the primary purposes of the experiment was to induce the bend–twist coupling, the mounting structure must not significantly move or flex as this would change the

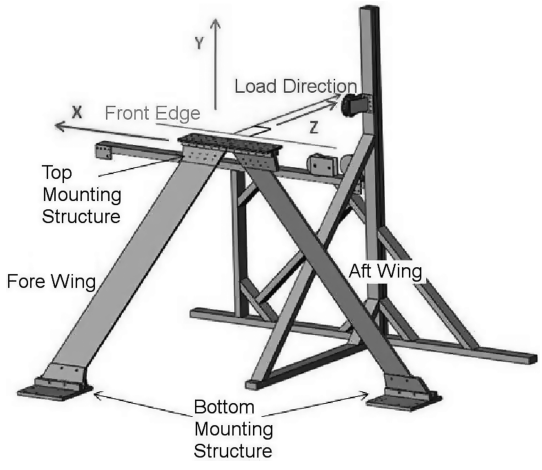

Fig. 4 Joined wing with loading structure and loading direction.

geometry of the test article and possibly negate the bend–twist coupling. Any movement of the base was recorded for use in future validation efforts and to quantify the error induced by the necessary flexibility to avoid stress concentrations which would have led to premature failure unrelated to the bend–twist coupling.

The load was applied in the same manner as the qualification test article, approximately perpendicular to the front edge of the joined wing's top mounting structure and between the top of the joined wing and the top pulley, which was approximately horizontal, as shown in Fig. 4.

3. *Loading Structure*

The loading structures, as shown in Figs. 3 and 4, were required to be able to load the qualification and joined-wing test articles, respectively, with a known and repeatable load, roughly perpendicular to the test article. This point load was an approximation for the load due to lift on the wing. There were two loading structure configurations for this project: qualification and joined wing. The loading structures were anchored to the floor with concrete anchors at multiple locations to keep the loading structures from moving under load.

4. *Measuring Displacements and Rotations*

The FARO Photon 80 laser scanner was used to record displacements of the test articles under various loads. The FARO Photon 80 laser scanner was designed as a room or a large object scanner. The Photon 80 records the reflectivity of the surface and can distinguish between white and black. Being able to distinguish black from white was helpful in identifying various points on the test article as reference points as well as FARO provided targets. These targets aided in data reduction and correlation by allowing the scans to be aligned to each other even if the scanner was moved. The FARO Photon 80 recorded the data as a set of points.

The FARO laser tracker was used to more precisely record point deflections. The accuracy was significantly greater than the FARO Photon 80, 0.0008 in. compared with 0.03 in. The spherically mounted retroreflectors (SMRs), which the laser tracker tracks in three dimensions, can be put in a known and specific location on the test article. This point was then measured and compared with the corresponding point in the FE model.

To create consistent data sets, several basic steps were performed: initial zero scans, intermediate low load scans, and final zero scans. The initial zero scan was the baseline for deflection measurements. Because of the weight of the load cell and cable, the zero scan was taken without these attached. Between each load case, the test articles were unloaded to a relatively low but repeatable load and rescanned. If there was any permanent deformation or slipping in the mechanical joints from the previous load case, the deflection would show up in the scan and all subsequent data could be corrected by this offset. At the end of a set of load cases, the test article was again returned to a zero load state by removing the cable and was scanned. In addition to laser scan data, several other data sources were recorded: the strain, applied load, direction of the load, and the height of the pulley.

B. Analytical Models

FE models were created and their results were analyzed and compared with measured data both before and after the experimental testing. Before testing, FE models were used in the experiment design process. After the testing, the FE models were hand tuned to match the measured displacement and strain data. Tuning the FE models was easiest for the qualification models, and lessons learned from the qualification tests were applied to the joined-wing models. These lessons learned helped in the design of the joined-wing test article and reduced the risk of designing the joined-wing test article incorrectly.

For all the FE models, several versions of Nastran were used interchangeably: MD Nastran V2007.0, MD Nastran V2008.0, and NX Nastran V5.0. MD Nastran V2007.0 was the primary solver for most analyses. For all linear analyses, solution method 101, SESTATIC, was used. For all nonlinear analyses, solution method 106, NLSTATIC, was used. QUAD4 plate elements were used exclusively to represent the various parts of the test articles. The qualification and joined-wing test articles were modeled separately, and the mounting structures were modeled as well. The primary assumptions going into the FE modeling process were that the material was homogeneous and isotropic, the floor was a rigid boundary constraint, and that the top and bottom connector bolts acted like six-degree-of-freedom spring elements.

1. *Linear and Nonlinear Solutions*

When computing FE static displacement solutions, static solvers fall into two main categories: linear and nonlinear. The fastest and easiest solutions come from the linear solver. The assumption of linearity significantly reduces the computations required when compared with nonlinear assumptions and allows the analysis to be solved in a single simultaneous equation set. However, linear solutions only agree with the measured results when deflections are small, since beyond small deflections, the linear assumption does not apply. A nonlinear solver must therefore be used for large deflections. The bend–twist coupling seen in the test articles, especially the joined-wing test article, must also be solved with a nonlinear solver since bend–twist coupling is an inherently nonlinear effect.

Because of the issues and approximations involved in creating FE models, accurate data is vital in validating modeling approaches. Significant effort has been spent on creating faster ways of computing nonlinear solutions for the joined wing, especially for the purpose of optimization. Because of the bend–twist coupling of the joined wing, time-prohibitive nonlinear optimizations must be used for accurate predictions. Therefore, various new techniques have been developed, including GEBT. Such new or hybrid techniques need accurate experimental data to use in validation for them to be considered valid and trustworthy methods.

2. *Reducing the Data*

The most significant challenge with the data recorded was that the coordinate systems of the scanner systems and FE model were not the same. Therefore, the scanner and tracker coordinate systems were aligned to the known FE model geometry.

This alignment required a two-step process. Known geometry on the test article's bottom mounting structure was scanned with the laser tracker for aligning the laser tracker coordinate system with the FE models. Spherical targets around the testing area were also scanned with the laser tracker. These were used to align the Photon 80's coordinate system with the FE model, since the lower accuracy of the Photon 80 made it difficult to locate the mounting structure's features.

After the data had been oriented to the correct coordinate system, the Photon 80 scan points, a collection of thousands of individual measurement points, were converted into a surface mesh. From the mesh, a surface was lofted. This lofted surface was then imported directly into the FE modeling postprocessor for visual comparison of the surface shape.

This surface was sliced into several sections. The end points of these sections were compared with the closest node in the FE model. This node was determined by selecting the corresponding points between the undeformed model and unloaded test article surface. The distance between these corresponding points was calculated and all the distances were averaged together using:

$$\text{ADE} = \frac{\sum_{i=1}^{n}\left(\sqrt{(g_{x,n}-s_{x,n})^2+(g_{y,n}-s_{y,n})^2+(g_{z,n}-s_{z,n})^2}\right)}{n} \tag{2}$$

where ADE is the average distance error, g_x is the x-direction position of the grid point, g_y is the y-direction position of the grid point, g_z is the z-direction position of the grid point, s_x is the x-direction position of the surface point, s_y is the y-direction position of the surface point, s_z is the z-direction position of the surface point,

and n is the number of grid points (16 for the qualification model and 26 for the joined-wing model). This resultant number, the ADE, gave a quick feel of how well the surface shape matched the FE model; the larger the number, the worse the correlation.

After the previously described alignment, the laser tracker's point data were then directly compared with the same location in the FE model, and plots of deflections were created.

IV. Results and Analysis

A. Material Properties

The modulus of elasticity of the 6061 aluminum used in the wing segments was measured at 9.9E6 psi, which agreed closely with other reported values [19]. This modulus was used in all the FE models. Five samples were tested in the MTS tensile test system. Yield was recorded to be around $4500\mu\epsilon$. To include a margin for error with respect to permanent deformation of the test article, $4000\mu\epsilon$ was used as the yield limit and was never exceeded as measured at all strain gauge locations. This margin also took into account that the strain gauges may not be at the highest stress locations even though the gauges were placed at or as close as possible to the highest stress locations.

B. Qualification Test Article

All qualification test article data is been transformed so that the following coordinate system is used: x is in the forward direction or direction toward the front of the notional aircraft, y is out of the wing tip, and z is in the load direction or upward with respect to the notional aircraft; as shown in Fig. 5. The qualification test article was loaded along both bending axes as explained in Sec. IV.B.1.

1. Load Deflection Curves

Lateral Bending. With the laser tracker, a tracker point was measured near the top of the test article, as shown in Fig. 6. There were four data sets of the measured displacements of the point: x, y, and z displacements with load and the root-mean-squared (rms) or total displacement. Load deflection curves for y and z displacements with load were plotted in Figs. 7 and 8. The x displacement was negligible (less than 0.001%) and the RMA was dominated by the z displacements, as this was the greatest displacement. The diamonds represent the experimental results; the solid line represents the nonlinear FE model solution; and the dashed line represents the linear FE model solution. The displacements have been non-dimensionalized by the length of the beam, 72 in.

While the measured data was in close agreement to the nonlinear FE models, the y- and z-direction error was due to the change in load direction in the test article, because the load application point was fixed and the test article deflected through a large angle. In the FE model, the load was assumed to stay along the z direction. While the actual load direction could be simulated, the agreement shown was close enough for this data. It is also worth noting that the beam was extremely flexible; at 200 lb load, the beam had deflected 28% of its 72 in. length.

Fig. 6 Qualification: lateral bending, tracker point.

Transverse Bending. A tracker point was measured near the top of the test article, as shown in Fig. 9. There are four data sets of the measured displacements of the point: x, y, and z displacements with load and the rms or total displacement. The load deflection curves for the x and z displacements are plotted in Figs. 10 and 11.

Agreement between predicted and measured displacements in the transverse bending test was not as good as the lateral bending test for several reasons. First, alignment was difficult because of software incompatibilities, as explained in the lateral bending section; and second, the applied force was not along the z direction. The applied force was angled 4 deg toward the x axis because the load application structure was oriented for the lateral bending qualification test and could not be moved to properly align with the load point. This added an extra layer of complexity to the FE model. A loading structure that could adjust the load direction would be required to improve correlation.

2. Surface Matching

Lateral Bending. For the qualification test article, the FE models could easily be tuned using the surface data from the Photon 80. It was hoped that these tuned values would work well as a first-order approximation of the needed values for the corresponding joined wing. As will be discussed in the upcoming joined-wing section, this was not the case. The tuning of the qualification model was not a

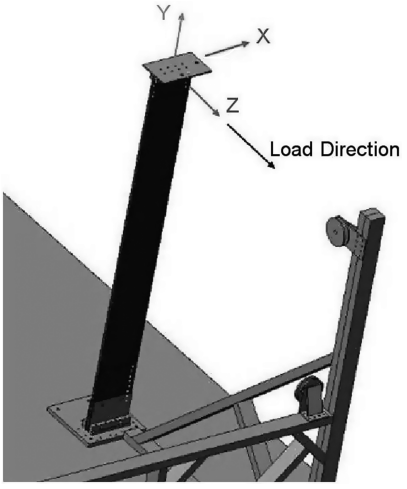

Fig. 5 Qualification coordinate system.

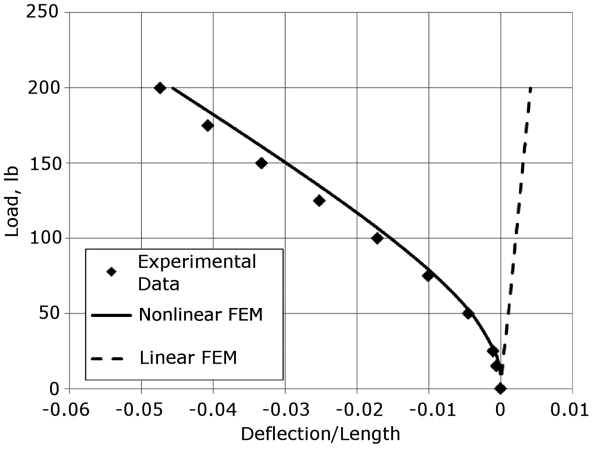

Fig. 7 Qualification: lateral bending, *Y* direction.

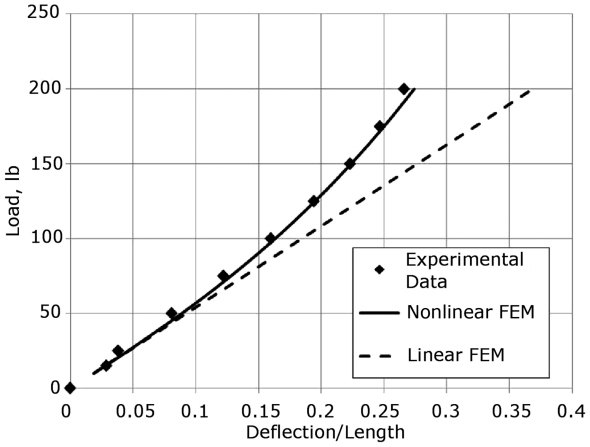

Fig. 8 Qualification: lateral bending, *Z* direction.

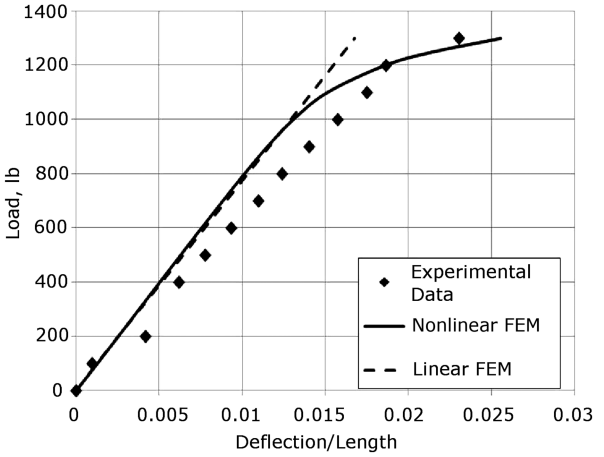

Fig. 11 Qualification: transverse bending, *Z* direction.

wasted activity; it provided needed experience for quickly tuning the joined-wing model.

For the initial alignment between the scanner and FE coordinate systems, the unloaded structure had an ADE of 0.034. For the 150 lb load case, the nonlinear solution, Fig. 12b, had an ADE of 0.19 in. and the linear solution, Fig. 12a, had an ADE of 1.75 in. The nonlinear FE model predicted displacements which closely matched the measured displacements at 16 points along the surface, showing that the overall surface shape was matched. This validated the method of scanning and recording the test article as well as method of matching the surface shape in the FE model with the test article, providing a link between analytical and experimental data which went beyond just tip displacement. This becomes much more important with the joined-wing test article as surface shape is an important feature to calculate in the FE model when predicting bend–twist coupling.

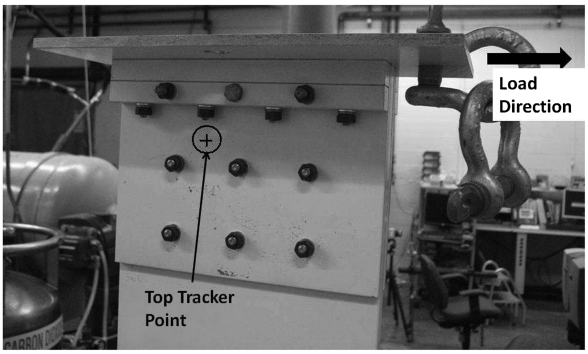

Fig. 9 Qualification: transverse bending, top tracker point.

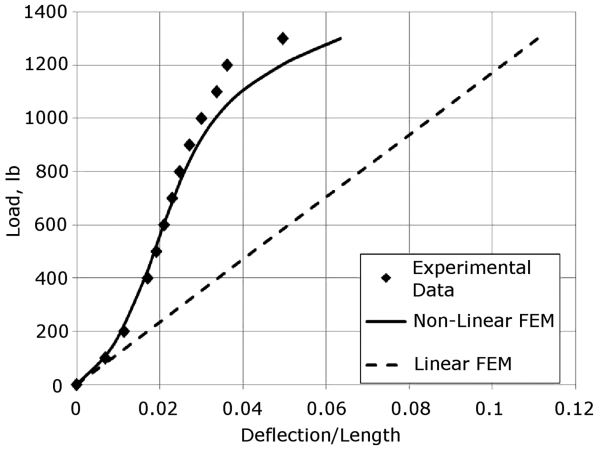

Fig. 10 Qualification: transverse bending, *X* direction.

Transverse Bending. For the initial alignment between the scanner and FE coordinate systems, the unloaded structure had an ADE of 0.0009. For the 1000 lb load case, the nonlinear solution, Fig. 13b, had an ADE of 0.32 in. and the linear solution, Fig. 13a, had an ADE of 1.35 in. This showed that for this type of loading, a nonlinear solution was required. A twisting was also seen but not shown here, signifying that the beam was buckling as expected.

3. *Strain*

Lateral Bending. As shown in Fig. 14, there are three strain gauges on the qualification test article. Gauges 1 and 2 are on the front surface of the beam and gauge 3 is on the side, approximately on the neutral axes of the thin side of the beam. The recorded strains are shown in Fig. 15. Gauges 1 and 2 track together as expected, which signifies that the test article was not twisting about the *y* axis as it was loaded. Low values of strain were recorded at gauge 3, which signifies that the gauge was not exactly on the neutral axis of the beam.

Transverse Bending. When the qualification test article was loaded such that it bent about the *z* axis, the resulting strain, as shown in Fig. 16, indicated the expected buckling. At the low load levels, the recorded strains in gauge 1 indicated increasing compression and the recorded strains in gauge 2 indicated increasing tension. After 900 lb, the strain values in gauge 1 changed from increasing to decreasing. This change indicated the onset of the beam buckling, as the beam started rotating about the *y* axis. It was predicted in Eq. (1) that buckling would occur at 1000 lb. The earlier buckling was due to the load angle error as explained in Sec. IV.B.1 above as well as a difference in the boundary constraints of the test article compared with the assumption in the mathematical equation. This error was acceptable for this experiment because this was not the primary research.

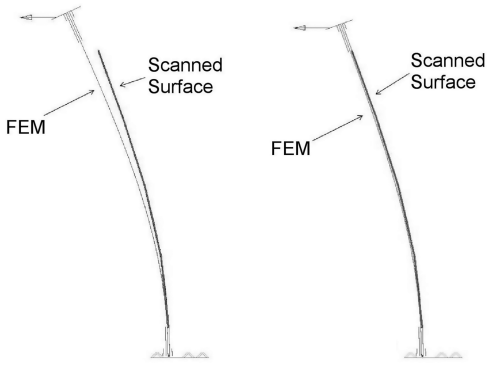

Fig. 12 Qualification: lateral bending, 150 lb surface matching: a) linear and b) nonlinear.

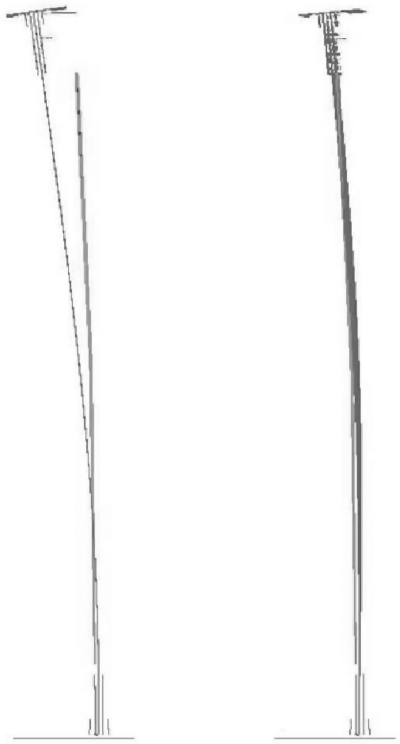

a) b)

Fig. 13 Qualification: transverse bending, 1000 lb surface matching: a) linear and b) nonlinear.

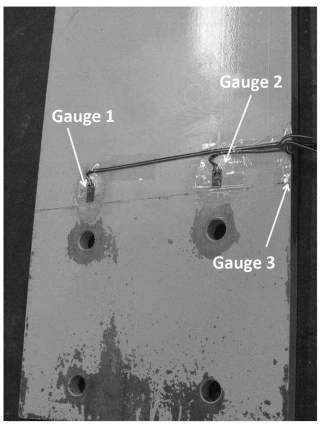

Fig. 14 Qualification test article with gauges.

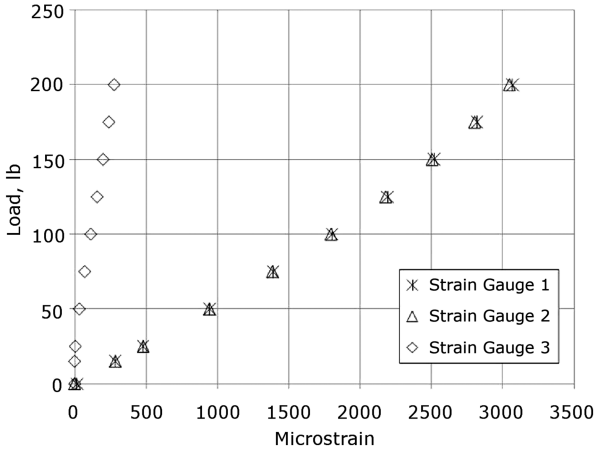

Fig. 15 Qualification: lateral bending, recorded strain.

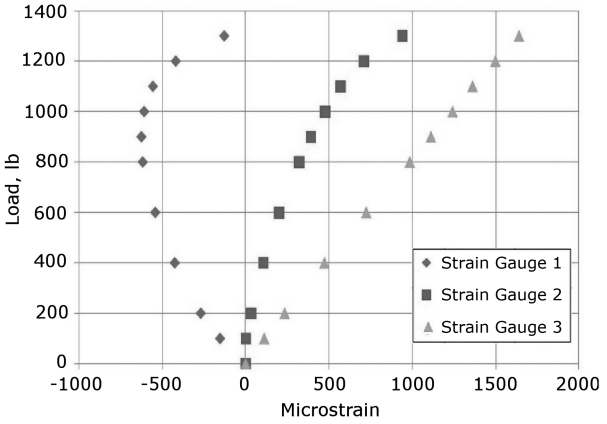

Fig. 16 Qualification: transverse bending, recorded strain.

C. Joined-Wing

The joined-wing test article was designed with the express purpose of clearly demonstrating the nonlinear bend–twist coupling inherent with the joined-wing design, as described previously. Three data sets were collected during the experiment using the laser systems: top deflections (laser tracker), surface shape (Photon 80), and base movement (laser tracker). The strains, load angles, and structural angles as select locations were also recorded. All data was transformed so that the following coordinate system was used: x was in the forward direction or direction towards the front of the notional aircraft, y was out of the wing tip, and z was in the load direction or upward with respect to the notional aircraft; as shown in Fig. 4.

For the FE model, the stiffness coefficients from the qualification model were used as a starting point for the stiffness coefficient values in the joined wing. These values produced a joined-wing FE model that was not significantly rigid when compared with measured responses. Therefore, the qualification FE model coefficients were not used in the joined-wing FE models. Instead, the same trial and error method as used for the qualification FE models was used for the joined-wing FE models.

1. *Deflection Curves*

With the laser tracker, four points were tracked during the experiments. The locations of the points on the test article are shown in Fig. 17. Point 1 also shows the SMR at the point location. The points are offset 1 in. from the surface, which is the center of a mounted SMR.

The tuned FE model solutions agreed closely with the nonlinear range of the experimental results. All the displacement plots of this section use the following symbols: the diamonds represent the experimental results, the solid line represents the nonlinear FE model solution, and the dashed line represents the linear FE model solution. The displacements have been nondimensionalized by the length of the joined wing, 57 in.

There were four data sets of the measured displacements at each point: x, y, and z displacements with load and the rms or total displacement. At all four of the points, the x, z, and rms displacements were similar. The plots for x and z displacements, and rms displacement are shown in Figs. 18–20. These plots show that the solution most clearly matches the nonlinear solution, as expected. The z-direction FE model solutions and measured displacements agreed closely in the 300–1100 lb range ($\leq$ 5% error), since the FE model was tuned using this range of data. Displacements in the z direction represent the greatest change in movement, shown in the values and the fact that the rms values and error closely track the z direction, seen in Figs. 19 and 20.

The displacements in the y direction did not follow the same trend as the other directions. As shown in Figs. 21 and 22, the displacements varied between the two points on the end of the test article. This displacement had the poorest correlation, but the y values were also the smallest. Therefore, the error had the least effect on the

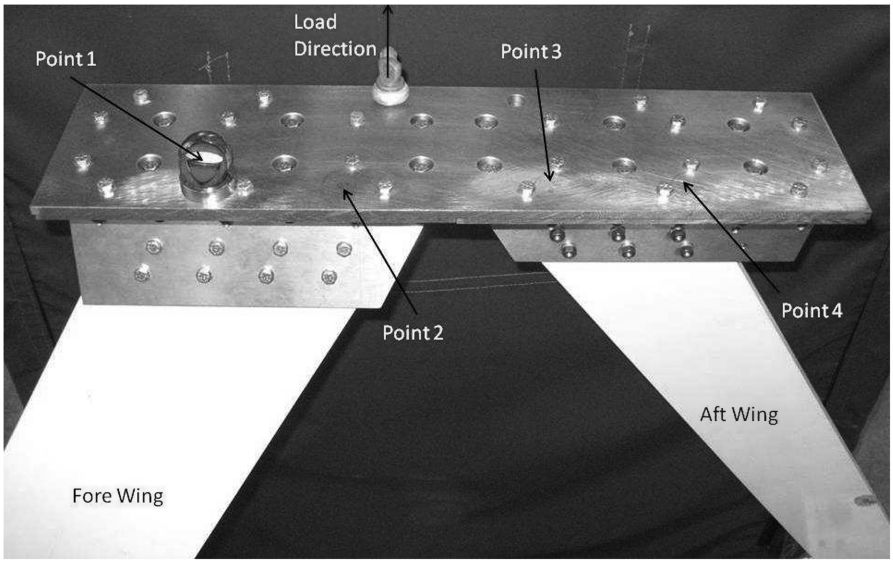

Fig. 17 Joined-wing tracker points.

overall deflection and shape of the FE model. These results showed that the top plate was rotating slightly as the test article was loaded.

It is important to note that the maximum translation at 1200 lb is only 6 in., or 11% of the test article's 57 in. height, compared with the 28% deflection at 200 lb for the qualification test article. This highlights one primary reason the joined-wing concept is being considered as a HALE aircraft design despite the complex geometric couplings; the joined-wing design is extremely stiff.

2. Surface Shape

The Photon 80 surface scanner data, in the form of lofted surfaces, was compared with the FE model to verify that the FE model was correlated. It is not sufficient to merely match the tip deflection when validating analytical codes for modeling the joined wing; the full bend–twist coupling must be evident and matched to determine if the FE model is indeed valid. For the initial alignment between the

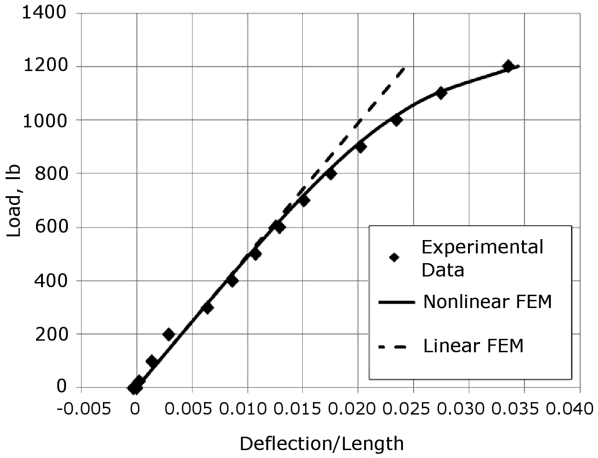

Fig. 18 Joined wing: *X* direction.

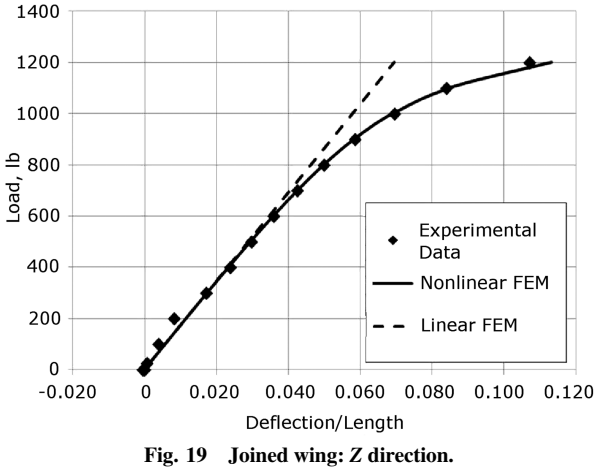

Fig. 19 Joined wing: *Z* direction.

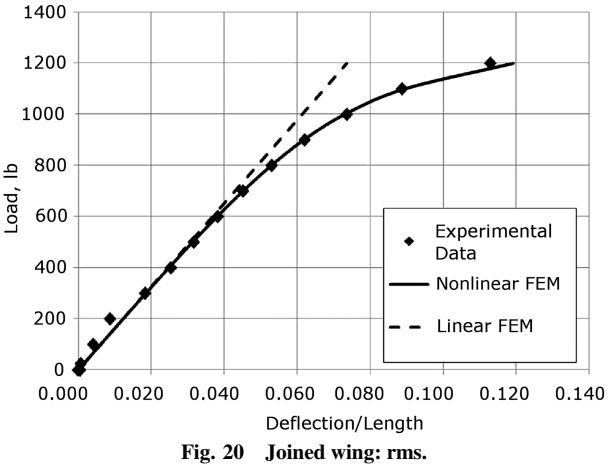

Fig. 20 Joined wing: rms.

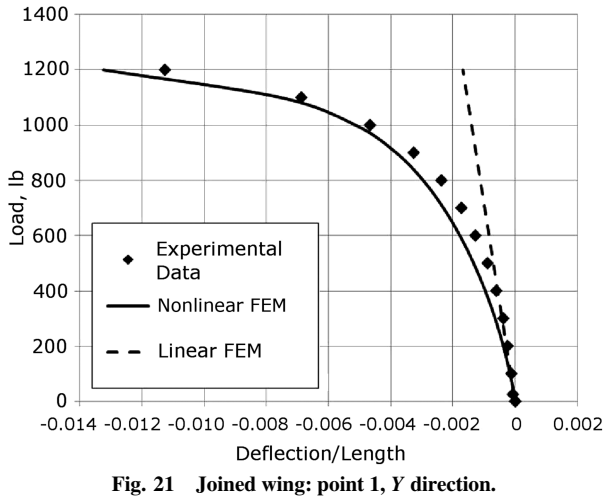

Fig. 21 Joined wing: point 1, *Y* direction.

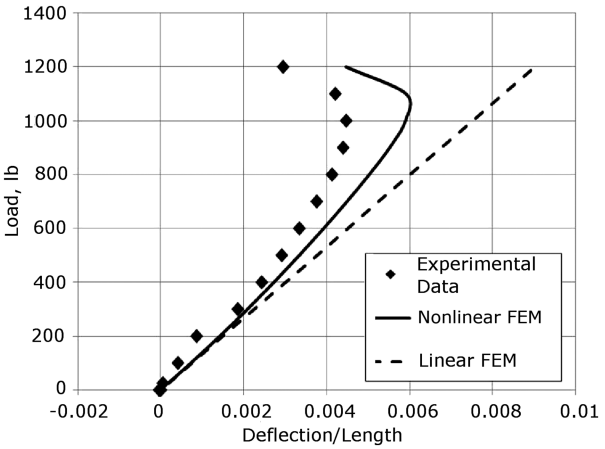

Fig. 22 Joined wing: point 4, *Y* direction.

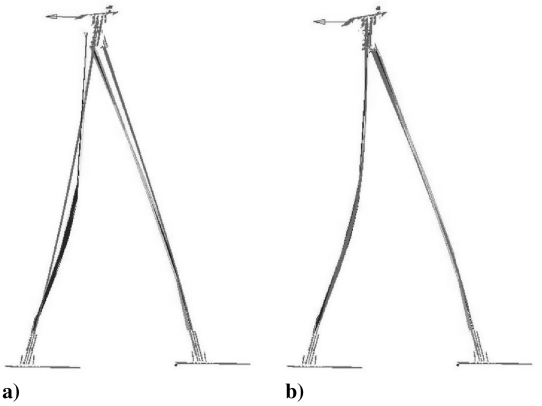

Fig. 24 Joined wing: a) linear and b) nonlinear FE model under a 1200 lb load.

scanner and FE coordinate systems, the unloaded structure had an ADE of 0.23.

Figure 23 shows the test article under a 1200 lb load. Figure 24 shows the linear (Fig. 24a) and nonlinear (Fig. 24b) FE model compared with the surface data. It is clear that the linear solution did not align well with the surface shape, whereas the nonlinear solution aligned quite well. The linear case had an ADE of 0.77 in., and the nonlinear case had an ADE of 0.18 in.

Figure 23 clearly shows the aft wing segment in a bend–twist deformation. This highlights that this joined-wing test article was designed correctly. The test article was loaded to 1200 lb three times and exhibited no permanent deformation.

3. Strain

On the test article, there were four strain gauges, shown in Fig. 25. The values recorded from these gauges during the experiment are shown in Fig. 26. It is worth noting that as the joined-wing test article began to act in a nonlinear manner, the values in gauge 3 begin to decrease. This was caused by the aft wing segment root experiencing a stress relief because of the bend–twist coupling. Figure 26 shows that the maximum load applied of 1200 lb was the last load case before material yielding, since the 4000$\mu\epsilon$ yield point would have been reached before 1300 lb.

Fig. 23 Joined wing: test article under a 1200 lb load.

4. Base Movement

One of the concerns with the design of the joined-wing test article was movement of the base plates. In the FE model, it was assumed that the base plates were constrained against all movement. In reality, this is, at best, a fairly good assumption. Therefore, several laser tracker points were evaluated at specific locations on the base plates, shown in Figs. 27 and 28.

The main reference points were 1 and 2 for both the fore and aft base plates. In general, the recorded data showed that while the base did move, the displacement were under 0.003 in. The only direction greater than 0.003 was in the *y* direction of the fore base plate reference points. This signifies that the base plate was lifting slightly

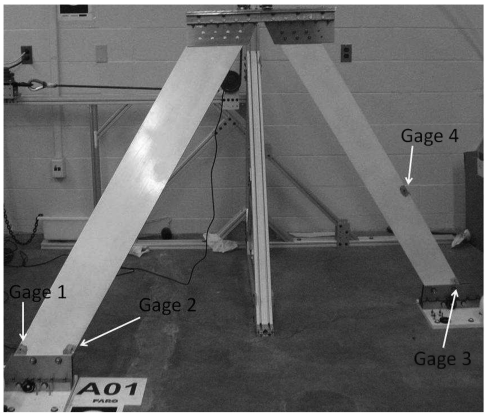

Fig. 25 Joined-wing test article with gauges.

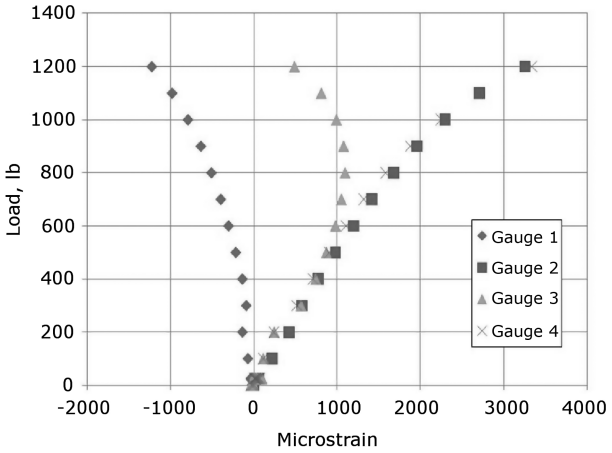

Fig. 26 Joined wing: recorded strain.

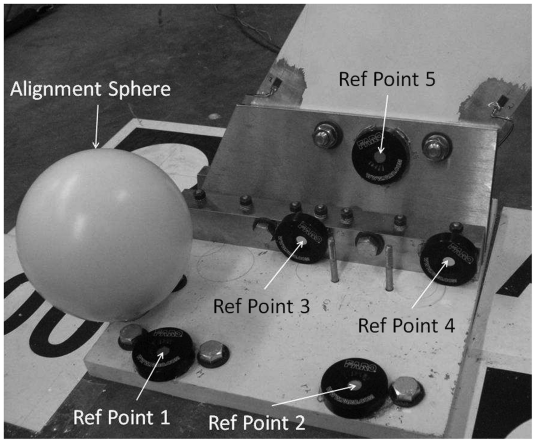

Fig. 27 Joined wing: fore base plate, reference points.

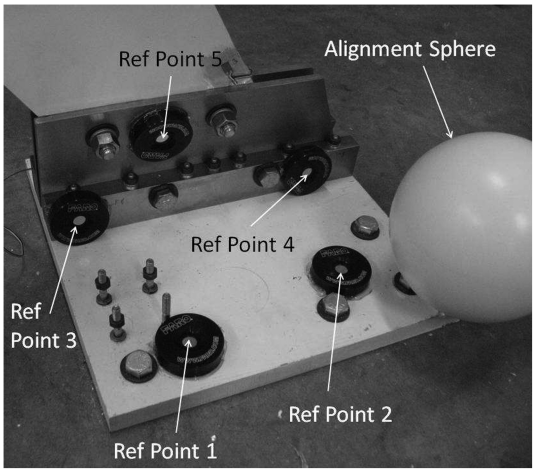

Fig. 28 Joined wing: aft base plate, reference points.

under high loads; however, this was still low enough that the assumption of no rotation was still valid, as the movement contributed to less than 2% error in tip deflection at a 1200 lb load.

V. Conclusions

The goals of this research were to provide experimental data on simple joined-wing test articles that will allow researchers to validate tools like GEBT for use in the design of joined-wing HALE aircraft, to develop a standard set of experimental procedures for testing joined wings in the lab, and to compare experimental data with analytical results. These goals were met: quality data was collected that is ready to use for optimization, the experimental procedures were verified and ready for further use, and the data were compared with preliminary FE models showing that nonlinear analyses are required for the joined-wing design.

The qualification test article was tested with respect to both bending axes. Preliminary FE models showed good correlation. Bending in the transverse direction produced the expected nonlinear geometric coupling.

The joined-wing test article was successfully tested. The test article was designed to exhibit nonlinear bend–twist coupling before material yield and this was clearly observed and measured. Even though the aft wing segment displayed the bend–twist coupling, it was still under the material yield point. The difficult design constrains of geometric nonlinearity coupled with material linearity were successfully realized. The FE model correlated well, although the FE model showed a higher amount of top plate rotation than the experimental results. The surface scans aligned with the FE model as the load was increased, matching the deflections in both the fore and aft wing segments as well as the bend–twist coupling. Strain measurements showed that during the nonlinear bend–twist coupling of the joined wing, the root of the aft wing experienced a stress relief.

The Photon 80 performed extremely well for capturing the surface shapes of the test articles. The laser tracker added the precision data needed to create accurate point tracks, verify that the base constraints were correct, and align the data to the FE model.

Besides a significant quality and quantity of collected data, the reason the joined-wing concept is popular for HALE aircraft, despite its complicated geometric nonlinearities, was shown: this design is extremely stiff. The qualification test article experienced 28% deflection compared with length at only a 200 lb load, whereas the joined-wing test article experienced only 11% deflection at 6 times the load. Further, at a 200 lb load, the joined-wing experienced $\leq 1\%$ deflection. This allows a similarly designed joined-wing HALE aircraft to devote significantly less structure to the wings to resist bending than in a single wing HALE aircraft.

Acknowledgment

The views expressed in this paper are those of the authors and do not reflect the official policy or position of the U. S. Air Force, U.S. Department of Defense, or the United States Government.

References

[1] Wolkovitch, J., "The Joined Wing: An Overview," *Journal of Aircraft*, Vol. 23, No. 3, 1986, pp. 161–178. doi:10.2514/3.45285

[2] Green, N. S., Canfield, R. A., Swenson, E., Blair, M., and Yu, W., "Structural Optimization of Joined-Wing Beam Model with Bend/Twist Coupling Using Equivalent Static Loads," *50th AIAA/ASME/ASCE/AHS/ASC Structures, Structural Dynamics, and Materials Conference*, AIAA Paper 2009-2644, Mar 2009.

[3] Yu, W., and Blair, M., "GEBT: A General-Purpose Tool for Nonlinear Analysis of Composite Beams," *51st AIAA/ASME/ASCE/AHS/ASC Structures, Structural Dynamics, and Materials Conference*, AIAA Paper 2010-3019, April 2010.

[4] Gallman, J. W., Smith, S. C., and Kroo, I. M., "Optimization of Joined-Wing Aircraft," *Journal of Aircraft*, Vol. 30, No. 6, 1993, pp. 897–905. doi:10.2514/3.46432

[5] Gallman, J. W., and Kroo, I. M., "Structural Optimization for Joined-Wing Synthesis," *Journal of Aircraft*, Vol. 33, No. 1, 1996, pp. 214–223. doi:10.2514/3.46924

[6] Roberts, R. W., Jr., Blair, M., and Canfield, R. A., "Joined-Wing Aeroelastic Design with Geometric Non-Linearity," *Journal of Aircraft*, Vol. 42, No. 4, 2005, pp. 832–848. doi:10.2514/1.2199

[7] Bond, V. L., Canfield, R. A., Cooper, J., and Blair, M., "Scaling for a Static Nonlinear Response of a Joined-Wing Aircraft," *12th AIAA/ISSMO Multidisciplinary Analysis and Optimization Conference*, AIAA Paper 2008-5849, Sept. 2008.

[8] Boston, J., Green, N. S., and Keller, N., "Mech 542 Aluminum Joined-Wing Experiment," Air Force Inst. of Technologies Final Report for Mech 542, 2009.

[9] Patil, M. J., "Nonlinear Aeroelastic Analysis of Joined-Wing Aircraft," *AIAA/ASME/ASCE/AHS Structures, Structural Dynamics, and Materials Conference*, AIAA Paper 2003-1487, April 2003.

[10] Marisarla, S., "Structural Analysis of an Equivalent Box-Wing Representation of Sensorcraft Joined-Wing Configuration for High-Altitude, Long-Endurance (HALE) Aircraft," M.S. Thesis, Univ. of Cincinnati, Cincinnati, OH, March 2005.

[11] Narayanan, V., "Structural Analysis of Reinforced Shell Wing Model for Joined-Wing Configuration," M.S. Thesis, University of Cincinnati, Cincinnati, OH, March 2005.

[12] Rasmussen, C. C., Canfield, R. A., and Blair, M., "Optimization Process for Configuration of Flexible Joined-Wing," *AIAA/ISSMO Multidisciplinary Analysis and Optimization Conference*, AIAA No. 2004-4330, Aug. 2004.

[13] Kaloyanova, V. D., Ghia, K. N., and Ghia, U., "Structural Modeling and Optimization of the Joined Wing of a High-Altitude Long-Endurance (HALE) Aircraft," *AIAA Aerospace Sciences Meeting and Exhibit*, AIAA Paper 2005-1087, Jan. 2005.

[14] Adams, B. J., "Structural Stability of a Joined-Wing SensorCraft," M.S. Thesis, Air Force Inst. of Technologies, June 2007.

[15] Omar, E., "Sensor Integration Study for Sensor Craft UAV Mid-Term Review," The Boeing Company Material Contract No. F33613-00-D-3052, Sept. 2003.

[16] Hodges, D. H., "A Mixed Variational Formulation Base on Exact Intrinsic Equations for Dynamics of Moving Beams," *International Journal of Solids and Structures*, Vol. 26, No. 11, 1990, pp. 1253–1273.
doi:10.1016/0020-7683(40)90060-9

[17] Yu, W., Hodges, D. H., Volovoi, V. V., and Cesnik, C. E. S., "On Timoshenko-Like Modeling of Initially Curved and Twisted Composite Beams," *International Journal of Solids and Structures*, Vol. 39, No. 19, 2002, pp. 5101–5121.
doi:10.1016/S0020-7683(02)00399-2

[18] Hartog, J., *Advanced Strength of Materials*, McGraw–Hill, New York, 1952.

[19] Chairman, M.-H.-. C. A., *Metallic Materials and Elements for Aerospace Vehicle Structures*, U.S. Dept. of Defense, MIL-HDBK-5H, 1998.